Vol.2019-CG-176 No.7
Vol.2019-DCC-23 No.7
Vol.2019-CVIM-219 No.7
2019/11/7

Biological Modeling of Feather Based on Morphogenesis

Jiajun Zhang[1,a)] Takashi Kanai[1,b)]

Abstract: Feather is a delicate structure with massive fiber curves (called *barbs*) branching out from a shaft. Its biological morphogenesis of feather follicle is decisive to diversify feather appearance. Modern CG tools construct feathers using NURB-curve related parameters to directly approximate the feather outlook, which is straightforward and user-friendly. However, without considering internal growth facts, it requires much user efforts to reproduce feather characteristics and lacks potentials to cover all types of feather. In this paper, we summarize recent morphogenesis studies and propose a new modeling scheme by emulating the feather growth into three stages: *Helical Growth* stage for barb generation, *Unfurling* stage for barb flattening and *Expansion* stage for barb adjustment. Since our approach follows real-world feather development, it is expected to procedurally guarantee common feather characteristics and be more flexible to extend to different types of feather under a unified scheme.

1. Introduction

Feather, like hair and fur, is one of the most noticeable skin appendage can be found in nature. However, unlike hair that can be represented by a single strand or fur that can be rendered as offset shells on a surface [9], feather holds a highly complex structure with hierarchical branches, which is insufficient to describe by a simple geometric primitive. Simply speaking, a feather has a stiff shaft (called *rachis*) at the middle, hundreds of *barbs* attach themselves on the shaft and interlock (called *barbules*) adjacently one by one to form two blades at macroscopic level.

In order to model such a structure, NURB-curves are frequently used to define shaft, barb curve, outline of two blades along with various control parameters in modern CG softwares. Artists can adjust control points of curves to directly approximate curvature of feather barb template and blade width along the shaft, then actual feather barb curves are generated based on user-defined template with the restriction of blade width. The shaft is often modeled as a radius-changing cylinder bending based on template, and the final output is the combination of two parts described above.

Such approximate modeling scheme is straightforward but have few connections to the real process of feather growth. Indeed it has taken the biological topology of a mature feather into consideration, however, the possible factors that may have decisive effects on the final feather shape and barb pattern are hidden inside the morphogenesis of feather follicle, thus these factors are then lost and undiscussable under this scheme. This may also be the reason of the loose correlation between blade outline and barb curvature on this kind of output, which is not the case for real feathers. Another limitation of this scheme is its specialization for wing feather modeling, seldom of its variants can handle other types of feather rather than wing feather.

In this paper, we present a novel modeling scheme that faithfully follows the process of feather morphogenesis, abstracts the concepts and phenomena during the feather development and maps them into different processes to emulate one feather growth cycle. Our scheme first defines feather follicle sheath geometry and growth parameters to generate barb curves and shaft from top to bottom. We then emulate the unfurling process of feather out of the sheath and adjust barb curves by considering the interlock between them.

By exploiting feather morphogenesis, we expect to provide a new perspective on biologically accurate feather modeling and a platform to discuss the possibility of feather animation and mechanical properties at microscopic level. This paper is also expected to be a bridge between biology and computer graphics and an applicability test of porting biological knowledge into feasible CG technologies.

The rest of this paper begins with a brief discussion of past feather modeling methods in Section 2, then follows an elaborate summary of two aspects of biological research in Section 3: feather structure and feather morphogenesis. Section 4 explains the mapping from biology knowledge to feather growth emulation and the details of new modeling scheme. We show the progress of the implementation of our modeling scheme in Section 5. At last we discuss the potentials, limitations and future work in Section 6.

2. Related Work

The first attempt at modeling feather may be traced to Dai et al.'s work [5] in 1995. By the inspiration of branching of plants, they define a set of parameters such as barb length and initial barb angle, with the combination of user-defined quadratic functions to propagate subsequent orientation of line segments for one barb and finally the whole feather blades. However, their work only focuses on Galliformes family feathers, and quadratic func-

[1] The University of Tokyo, 3-8-1 Komaba, Meguro-ku, Tokyo 153-8902, Japan.
[a)] zhang-jiajun@g.ecc.u-tokyo.ac.jp
[b)] kanait@acm.org

© 2019 Information Processing Society of Japan

tion seems not to be ideal for representing the barb curvature of mature feathers.

Chen et al. [3] proposed an impressive feather modeling and feather coats generation scheme. This development of feather structure is based on parametric L-system, which defines how segments of shaft and barbs should be generated step by step. Forces and randomness are also introduced to imitate the raggedness of feather, increasing the variety of output. NURB-curves are used to define the template of barb curve, which is also a limitation that all barb curves on the same side have an identical basis in spite of the randomness factors during their generation. Also their output is restricted to wing feather. Nevertheless, it is worth noting that they model the mesostructure between two barbs for BTF sampling so that the micro details of feather can be represented by rendering rather than direct modeling.

Another parameterized model proposed by Streit et al. [12] elaborately defines geometry properties for shaft and barb (length, width, angle, spacing, etc.). Instead of using single identical template, user can insert multiple key barbs represented by Bézier curves along the shaft at one side and interpolate between them to generate the whole blade. This approach removes the need of explicit definition of feather outline and is more flexible for editing. In the same year, Franco et al. [8] independently presented a similar approach, but unlike the previous one, two Bézier curves are served as outline, and automatically generate randomized control points of Bézier curve rather than defining key barb from user.

Recently, Baron et al. [1] have proposed a data-driven approach that is able to achieve biological accuracy in some aspects. Although the underlying barb curve construction is a variant of Franco et al.'s method, they use image analysis on real feather atlas to extract outline and shaft curve, which results in a more realistic feather outlook. However, because of the absent analysis on barb curves from atlas, the correlation of outline and barb curvature is not guaranteed. We also doubt the ability of extracting outline from the feather types with low barb density using this approach.

3. Background

3.1 Feather structure

A feather possesses three primary components: the *rachis* is the shaft of a feather with massive *barbs* branching out from its two sides, and similarly, a barb also has massive *barbules* at two sides as shown in Figure 1. The distal barbules on some barbs may have hooklets that hook the proximal barbules with curved margin on adjacent barb, which fasten all barbs as a whole: left and right *vanes* [17]. The existence of hooklets and curved margin on barbules is the key factor causes the distinction between flight feather and down feather, and between upper (pennaceous) part and lower (plumulaceous) part of contour feather [11].

3.2 Feather morphogenesis

Morphogenesis, a biological term used to specify the formation of feather at cellular level, takes place inside feather follicle on bird skin. Feather follicle is a cylindrical tissue that emerges by elongation and invagination from flat skin's epidermis layer [14][2] (Figure 3). Follicle collar, the region with ring cross section at the base of feather follicle formed by the invagination, holds stem

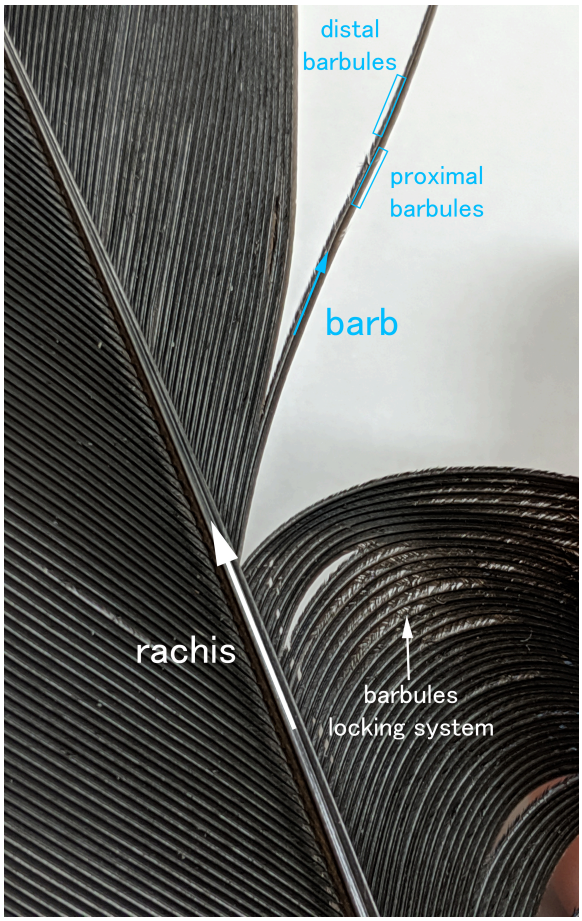

Fig. 1 A wing feather from Crow with its right vane split by hand. **Distal**: the anatomical orientation towards the tip; **Proximal**: the anatomical orientation towards the root.

Fig. 2 A contour feather from Pigeon. The barbs at the lower part hold simpler and longer barbules than the ones at the upper part, thus they cannot form vanes and become fluffy.

cells (pink squares in Figure 3) that actively proliferate and move upward, when cells arrived a thin horizontal area called *ramogenic zone* beneath follicle sheath, they start to differentiate and form rachidial ridge and barb ridges [13][2]. Therefore, the branching of feather does not proceed from bottom to top like plants but in a reverse direction; the tip of feather is formed first as barb ridges start to grow at ramogenic zone, differentiated successor cells add and rearrange themselves at the proximal end of each barb ridge causing the elongation of barb ridge.

About the feather type, if this cell rearrangement preserves the parallel of barb ridges, all barb ridges are radially symmetric and joint directly to collar, which causes the formation of fluffy *down feather* as Figure 3 **A**. If the rearrangement is towards one side

© 2019 Information Processing Society of Japan

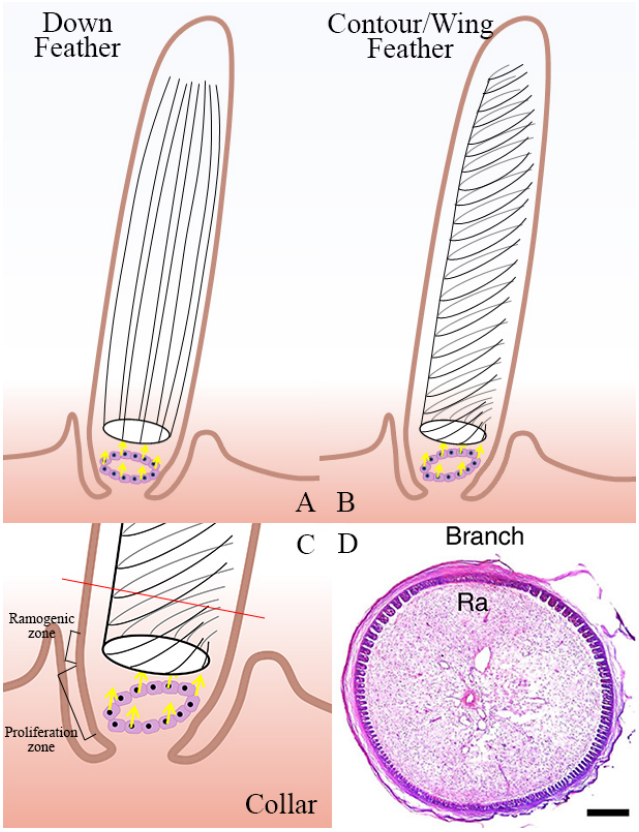

Fig. 3 An overview of feather follicle structure. Drawings are based on the knowledge from Yue et al. [15]. **(A)** Schematic drawing of a developing down feather follicle, which shows the parallel arrangement of barb ridges (black stripes). **(B)** Schematic drawing of a developing contour of flight/wing feather follicle, which shows the helical arrangement of barb ridges (black and gray curves). **(C)** A zoom-in of follicle collar. The proximal end of barb ridges are started to form after cells reach ramogenic zone. **(D)** A common real horizontal cross section of feather follicle at the level of red line in **C**. The **Ra** shows the locus and width of rachidial ridge at anterior polar, barb ridges lie on the circumference and continuously emerge from the *barb generative zone* located at posterior polar. This image **D** by Cheng et al. [4] is licensed under CC BY 4.0. Unmodified from original.

(anterior polar) of feather follicle, all barb ridges are bilaterally and grow helically beneath follicle sheath and fuse their proximal end to form the rachidial ridge (the **Ra** in Figure 3 **D**), which causes the formation of all feather types with shaft such as *contour feather* as Figure 3 **B**.

Furthermore, in the case of helical growth, new barb ridge emerges at the opposite side (posterior polar) where the barb generative zone is. If this posterior polar is biased, the distance that barb ridge will travel on the left and right half of collar will be not equal, which causes the vane width asymmetry of *flight/wing feather* [13][6][2], which is an important characteristic for flying.

Considering one regenerative cycling of a feather with shaft consisting of two primary phase: growth and resting phase [16]. In growth phase the elongation of follicle and helical growth of barb ridges are involved. When follicle becomes mature and its sheath starts to break, mature barbs with barbules developed inside barb ridges and with rachis developed from rachidial ridge are pushed out from the tip of sheath, and then unfurl themselves from helical to flat form. When moving to resting phase, the size of feather follicle shrinks and the cell proliferation is reduced [2], which causing the formation of proximal part of feather shaft which has no barb attached [16]. The posterior side of follicle sheath will eventually break to release all mature barbs out.

It is worth noting that the helical angle θ formed when a barb ridge fuses into rachidial ridge inside follicle may have significant difference from the angle A at the place where mature barb joint to rachis. Simultaneous with the unfurling of mature barbs, the mechanical properties of barbs and barbules locking state between barbs may cause an further expansion angle β for each barb, which has a noticeable effect on the final vane outline or even the pigment pattern on a feather [10]. See [6] for the reference of angles mentioned above.

4. Proposed Method

Based on the concept of being able to obtain the common biological characteristics of feather by faithfully following its biological growth activities, we propose a biological modeling scheme that procedurally generates feather vanes based on the facts mentioned in Section 3. We first emulate the basic morphogenesis of feather development in three stages: *Helical Growth*, *Unfurling* and *Expansion* to generate barb curves for two father vanes, then the rachis cylinder can be created via external CG modeling software based on the output of emulation.

4.1 Helical Growth stage

The first stage emulates the helical growth of barb ridges inside follicle. As the middle of Figure 4, we define the collar as a closed cycle $\boldsymbol{C}(s)$ parameterized by arc length percentage $s \in [0,1]$ in right-handed Cartesian space, mathematical representation (e.g. circle $\boldsymbol{Y}(s) = (\cos(2\pi s), \sin(2\pi s))$ or closed composite cubic Bézier curve can be used for this definition.

To simplify the discussion, we use the term *locus* to specify the 1D location s of an object on the collar $\boldsymbol{C}(s)$ and to discuss tangential movement later, we also use the *dot* "." to specify the properties of an object. We assume that the axis of collar is aligned with $+y$ axis, $\boldsymbol{C}(0)$ is located on $-z$ axis, and movement is said to be positive if it follows the clockwise direction, which will finally reach $\boldsymbol{C}(1) = \boldsymbol{C}(0)$. See left and right of Figure 4 for coordinates reference.

Just like rachidial ridge and bar generative zone segregating collar into left and right part explained in Section 3, anterior polar and posterior polar of collar are defined as two intervals I_A and I_P on $\boldsymbol{C}(s)$. Specifically, we denote the locus of two boundaries of one interval by a locus pair <left, right> specified by user, which corresponds to one of the boundary for left part and right part of collar (see left of Figure 4). Additionally, I_A should be guaranteed to include $\boldsymbol{C}(0)$, I_P is typically located around $\boldsymbol{C}(0.5)$ but is not mandatory.

Tangential Movement

To generate the distal end of each new barb, we define two moveable emitters E_l and E_r for the left and right side of $\boldsymbol{C}(s)$. As the left of Figure 4, each emitter starts moving from one boundary of I_A and spawns the distal end $P_0^{b_i} (i = 0, 1, \ldots)$ of the new i-th barb curve b_i at a frequency f, when it meets the same side boundary of I_P, its movement is clamped at the boundary but its spawning still proceeds.

© 2019 Information Processing Society of Japan

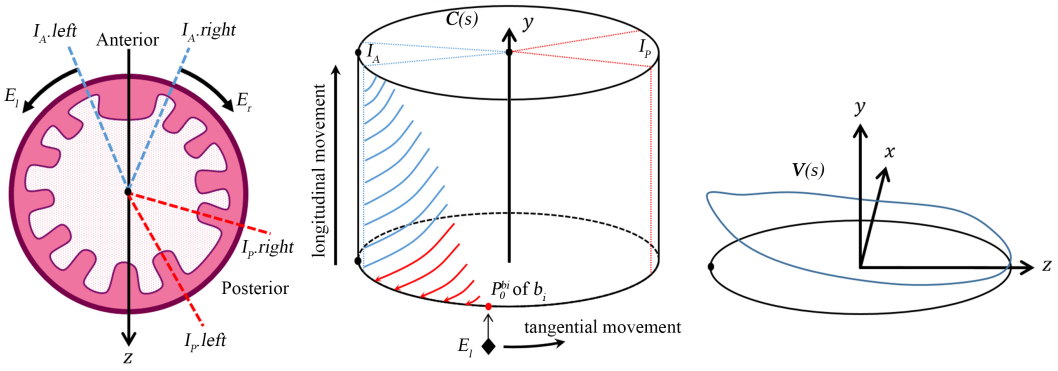

Fig. 4 **Left**: Schematic top view of $\boldsymbol{C}(s)$ in a follicle cross section style. The arrows indicate the tangential movement direction of E_l and E_r. **Middle**: Schematic drawing of the process of E_l in helical growth stage. Blue trails indicate the completed barbs. Red trails indicate the developing barbs. **Right**: An example of speed distribution $\boldsymbol{V_e}(s)$ or $\boldsymbol{V_b}(s)$ defined on $\boldsymbol{C}(s)$. Typically, the gradient of speed distribution should slant from anterior polar to posterior polar in order to match the curvature of convex tip and barb pattern of a feather. We also hypothesize that it may possibly be a reflection of concentration gradients of some chemical molecules reside in feather follicle [15].

The tangential speed of emitter movement on $\boldsymbol{C}(s)$ is defined by user as a speed distribution/gradient $\boldsymbol{V_e}(s)$ like the right figure of Figure 4. The definition approach is shown in Figure 6 and Figure 7. Therefore, the *locus* and the *spawn time stamp t* of $P_0^{b_i}$ can be calculated as:

$$\text{Left side: } P_0^{b_i}.\text{locus} = I_A.\text{left} - \int_{t=0}^{\frac{i}{f}} \boldsymbol{V_e}(s(t))dt \tag{1}$$

$$\text{Right side: } P_0^{b_i}.\text{locus} = I_A.\text{right} + \int_{t=0}^{\frac{i}{f}} \boldsymbol{V_e}(s(t))dt \tag{2}$$

$$P_0^{b_i}.t = \frac{i}{f} \tag{3}$$

To emulate the barb elongation, once a distal end $P_0^{b_i}$ of a new barb b_i is spawned, it starts moving just like emitter but in an opposite direction on $\boldsymbol{C}(s)$. After every time step, the locus of $P_0^{b_i}$ are recorded as the subsequent barb curve point $P_j^{b_i}(j = 1, \ldots)$. Its tangential speed is also defined by user as a speed distribution $\boldsymbol{V_b}(s)$ on $\boldsymbol{C}(s)$. When $P_0^{b_i}$ meets the boundary of I_P the elongation terminates and the generation of b_i is considered as completed (blue trails in the middle of Figure 4). The Equation (1) (2) can also be applied to calculate the locus of $P_j^{b_i}$ by replacing each term correspondingly, except its spawn time stamp can be directly assigned by the current time stamp (See Algorithm 1 for details).

Longitudinal Movement

Just like the new cells go from bottom to upward and push old cells higher, we emulate this activity as the longitudinal movement aligned to y axis. The scalar growing speed v_{grow} of feather follicle defined by user is used for the calculation of y coordinate of $P_j^{b_i}$:

$$y = v_{grow} * (t_{current} - P_j^{b_i}.t) \tag{4}$$

where $t_{current}$ denotes the current time stamp after the whole emulation starts. The calculation of longitudinal movement can be done after the tangential movement for simplification or simultaneously for real-time growth animation.

Termination & Coversion

The emulation can terminate when user-defined N barbs are completed, and all other developing barbs (red trails in the middle of Figure 4) are discarded. The x and z coordinate of $P_j^{b_i}$ are calculated by evaluating $\boldsymbol{C}(s)$ by $P_j^{b_i}$.locus. After all 1D barb curve points are converted into 3D vertice, the result is delivered into the next stage.

4.2 Unfurling Stage

The second stage emulate the flattening of each barb being pushed out of follicle sheath. When $P_j^{b_i}(j > 0)$ spawns, the binormal $\vec{n_j}$ of $\boldsymbol{C}(s)$ is calculated at $P_j^{b_i}$.locus as the rotation axis for line segment $\overrightarrow{P_j^{b_i} P_{j-1}^{b_i}}$ on the b_i. The unfurling rotation of one whole barb starts from distal end to proximal end, and the distal line segment $\overrightarrow{P_j^{b_i} P_{j-1}^{b_i}}$ is rotated around $\vec{n_j}$ to align the tangential

Algorithm 1: $P_j^{b_i}$ generation logic for left vane

```
External input: Current time stamp t_current from system
Function Update (Δt)
    /* Emitter movement and spawn */
    E_l.time ← E_l.time + Δt;
    // E_l.time is a temporary variable storing the
       accumulated time
    period ← 1/E_l.f;
    while E_l.time ⩾ period do
        E_l.time ← E_l.time - period;
        E_l.locus ← E_l.locus - period × V_e(E_l.locus);
        Check if emitter already meets boundary;
        Spawn the first point P_0^{b_next} for the next new barb curve b_next;
        P_0^{b_next}.locus ← E_l.locus;
        P_0^{b_next}.t ← E_l.t;
    end
    /* Barb elongation */
    foreach b_i generated by E_l do
        P_n^{b_i} ← the last point of b_i;
        if P_n^{b_i} has not met boundary then
            Spawn the next point P_{n+1}^{b_i} for barb curve b_i;
            timediff ← t_current - P_n^{b_i}.t;
            P_{n+1}^{b_i}.locus ← P_n^{b_i}.locus + timediff × V_b(P_n^{b_i}.locus);
            P_{n+1}^{b_i}.t ← t_current
        end
    end
```

© 2019 Information Processing Society of Japan

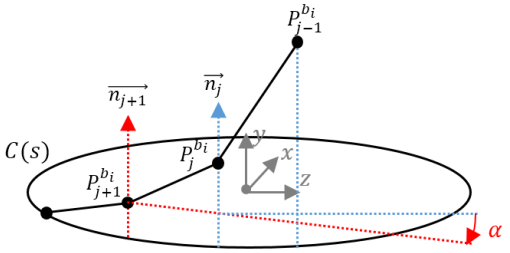

Fig. 5 Schematic drawing of unfurling process of barb b_i.

direction of the proximal line segment $\overrightarrow{P_{j+1}^{b_i} P_j^{b_i}}$. If we denote the angle of full alignment by α, then we can multiple an unfurling weight $w \in [0,1]$ to α to control the extent of each vane's unfurling.

4.3 Expansion Stage

The expansion phenomenon of barbs occurs simultaneously with the unfurling process but impact feather vane differently, thus we treat it as an individual stage. This additional curvature change of barbs is caused by both microscopic mechanical properties and the complex locking state of barbules which is dynamic and differs from feather to feather. We omit this part due to the lack of biological supports and mechanical analysis on the correlation between barbules and vane shape.

5. Results and Discussion

We have implemented the helical growth stage and unfurling stage of our modeling scheme using C++ and OpenGL. The real-time procedural generation of feather vanes are performed at 60 fps with the time step $\Delta t = 0.05$ sec., allowing the interactive detail adjustment during the generation.

Figure 6 shows a typical result of our implementation, the curvature of tip shape and barb pattern are controlled by the $\boldsymbol{V_e}(s)$ and $\boldsymbol{V_b}(s)$ respectively, both of these gradients slant to the locus $s = 0.5$ which is the position of posterior polar. Under this configuration, the output barb pattern correctly reflects a common characteristic that the inter-barb spacing around the edge of vane appear more compact than the one around the rachis (the lower barb pattern of Figure 6 at $t = 24$ sec.), which also matches the measurement data from Feo et al. [7] showing the incremental inter-barb spacing from distal end to proximal end of two barbs.

The abnormal barb density of tip part shown in Figure 6 is a known flaw caused by the dependency between spawning frequency f and speed of emitter, bound by the time. When emitter reach the posterior polar, its tangential component of displacement is lost so the density is also increased suddenly. This problem warns us the spawning strategy does not correspond to real biological activities, and we plan to fix it in the near future.

Figure 6 shows the control of vane width asymmetry by only moving the locus of posterior polar from 0.5 to 0.4 to 0.2. The change of the slope of tip slope and vane width correctly reflects the characteristic of asymmetric wing feather that the nearer a wing feather is located to the end of a wing, the narrower its distal vane (the leading edge) is, and the broader its proximal vane (the trailing edge) is [11].

6. Conclusions and Future Work

We have presented a novel feather modeling scheme by exploiting existing studies on microscopic biological activities inside feather follicle and by emulating real growth of feather. In our scheme, the helical growth stage handles and generates prototype of two feather vanes in a unified model, rather than independently defining geometric elements of feather shape without taking possible biological correlations into consideration. The tip shape of feather and the barb curvature are associated by the same longitudinal growth so that the relationship of feather outline and barb pattern can be preserved and be guaranteed to be biologically accurate in some degrees. The usage of follicle collar also guarantees the width scale between two vanes to be rational and blendable from one feather to another by simply moving the locus of posterior polar. The unfurling stage emulates the "hatching" of feather from follicle sheath, which provides space for user to adjust the curvature of the whole vanes yet still preserves the line representation of a feather rather than surface. This stage also provides the possibility to animate the growth process of a feather.

Another advantage of our scheme is the linkage to the microscopic biological studies, meaning that it has potential to transplant cellular pigmentation mechanism to texture feather without the dependence of real feather photos. It is also a better platform to study the physics simulation of barb-level movement of feather, as the geometric information of barbules hides inside barb ridges and can be biologically integrated into the process of helical growth stage.

However, this advantage is also our limitation because of the ambiguous information or the lack of research support of some phases during the feather morphogenesis, making some of our modeling process design infeasible. The abnormal spacing at the tip of our result is caused by the dependence of emitter's speed, which is further caused by the insufficient understanding of geometric development of early barb ridges. We plan to improve the spawning strategy of barb curves by further reviewing the related papers and taking barb ridge size into consideration.

The expansion stage highly relates to biomechanical studies including elastica of barbs and locking system of barbules, making it prospective but challenging to implement. In the future we would like to explore the biological studies about barbule mechanical properties to complete this stage.

References

[1] Baron, J. and Patterson, E.: Procedurally Generating Biologically Driven Feathers, *CGI2019: Advances in Computer Graphics*, Lecture Notes in Computer Science, Vol. 11542, Springer International Publishing, pp. 342–348 (2019).

[2] Chen, C.-F., Foley, J., Tang, P.-C., Li, A., Jiang, T. X., Wu, P., Widelitz, R. B. and Chuong, C. M.: Development, Regeneration, and Evolution of Feathers, *Annual Review of Animal Biosciences*, Vol. 3, No. 1, pp. 169–195 (online), DOI: 10.1146/annurev-animal-022513-114127 (2015).

[3] Chen, Y., Xu, Y., Guo, B. and Shum, H.-Y.: Modeling and Rendering of Realistic Feathers, *ACM Trans. Graph.*, Vol. 21, No. 3, pp. 630–636 (online), DOI: 10.1145/566654.566628 (2002).

[4] Cheng, D., Yan, X., Qiu, G., Zhang, J., Wang, H., Feng, T., Tian, Y., Xu, H., Wang, M., He, W., Wu, P., Widelitz, R. B., Chuong, C.-M. and Yue, Z.: Contraction of basal filopodia controls periodic feather branching via Notch and FGF signaling, *Nature Communications*, Vol. 9, No. 1, pp. 1–11 (online), DOI: 10.1038/s41467-018-03801-z (2018).

© 2019 Information Processing Society of Japan

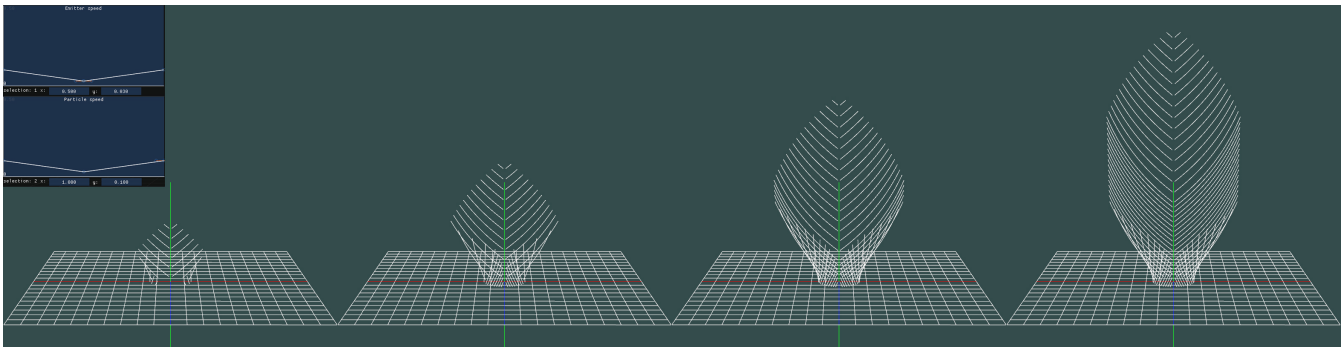

t = 6sec t = 12sec t = 18sec t = 24sec

Fig. 6 A generation sequence of a wing feather. $\boldsymbol{C}(s)$ is defined as a circle with radius 1.5 located at the origin. The same $\boldsymbol{V_e}(s)$ and $\boldsymbol{V_b}(s)$ are defined by using curve editing widgets shown at the top right of the first image, which are widely used in CG software like Blender. Notice that the time stamp t shows the progress of generation rather than the time consumed in real world. $I_A.left = 0.99, I_A.right = 0.01, I_P.left = 0.51, I_P.right = 0.49, f = 2.0$

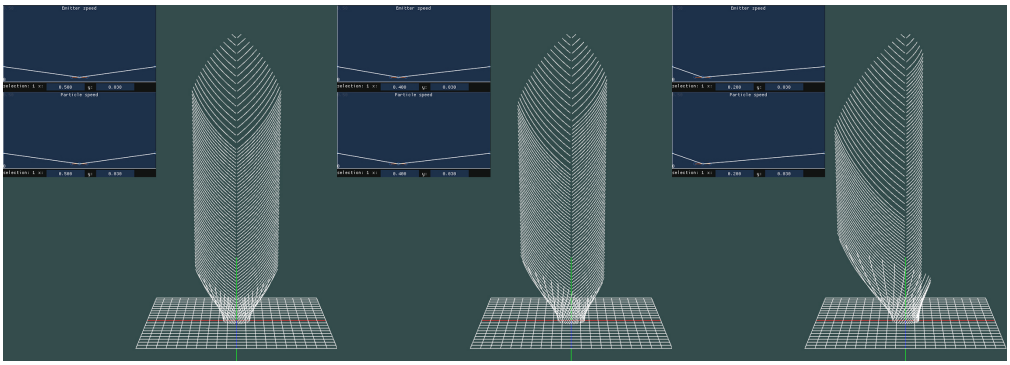

s_{polar} = 0.5 s_{polar} = 0.4 s_{polar} = 0.2

Fig. 7 Asymmetric blending of a wing feather at t = 42sec. The leftmost feather has the same configuration of Figure 6. The lowest point of $\boldsymbol{V_e}(s)$ and $\boldsymbol{V_b}(s)$ sync with the locus of posterior polar. $I_P.left = s_{polar} + 0.01, I_P.right = s_{polar} - 0.01, f = 2.0$

[5] Dai, W.-K., Shih, Z.-C. and Chang, R.-C.: Synthesizing Feather Textures in Galliformes, *Comput. Graph. Forum*, Vol. 14, No. 3, pp. 407–420 (online), DOI: 10.1111/j.1467-8659.1995.cgf143_0407.x (1995).

[6] Feo, T. J. and Prum, R. O.: Theoretical morphology and development of flight feather vane asymmetry with experimental tests in parrots, *Journal of Experimental Zoology Part B: Molecular and Developmental Evolution*, Vol. 322, No. 4, pp. 240–255 (online), DOI: 10.1002/jez.b.22573 (2014).

[7] Feo, T. J., Simon, E. and Prum, R. O.: Theory of the development of curved barbs and their effects on feather morphology: Theoretical Morphology of Curved Feather Barbs, *Journal of Morphology*, Vol. 277, No. 8, pp. 995–1013 (online), DOI: 10.1002/jmor.20552 (2016).

[8] Franco, C. G. and Walter, M.: Modeling and rendering of individual feathers, *Proc. XV Brazilian Symposium on Computer Graphics and Image Processing*, IEEE Comput. Soc, pp. 293–299 (online), DOI: 10.1109/SIBGRA.2002.1167157 (2002).

[9] Lengyel, J., Praun, E., Finkelstein, A. and Hoppe, H.: Real-time Fur over Arbitrary Surfaces, *Proc. Symposium on Interactive 3D Graphics*, ACM, pp. 227–232 (online), DOI: 10.1145/364338.364407 (2001).

[10] Lin, S. J., Foley, J., Jiang, T. X. and et al.: Topology of Feather Melanocyte Progenitor Niche Allows Complex Pigment Patterns to Emerge, *Science*, Vol. 340, No. 6139, pp. 1442–1445 (online), DOI: 10.1126/science.1230374 (2013).

[11] Lucas, A. M. and Stettenheim, P. R.: *Avian anatomy : integument*, U.S. Goverment Printing Office (1972).

[12] Streit, L. and Heidrich, W.: A BiologicallyParameterized Feather Model, *Computer Graphics Forum*, Vol. 21, No. 3, pp. 565–573 (online), DOI: 10.1111/1467-8659.t01-1-00707 (2003).

[13] Yu, M., Wu, P., Widelitz, R. B. and Chuong, C.-M.: The morphogenesis of feathers, *Nature*, Vol. 420, p. 308 (online), available from ⟨http://dx.doi.org/10.1038/nature01196⟩ (2002).

[14] Yu, M., Yue, Z., Wu, P., Wu, D.-Y., Mayer, J.-A., Medina, M., Widelitz, R. B., Jiang, T.-X. and Chuong, C.-M.: The developmental biology of feather follicles, *The International journal of developmental biology*, Vol. 48, No. 0, pp. 181–191 (online), DOI: 10.1387/ijdb.031776my (2004).

[15] Yue, Z., Jiang, T.-X., Widelitz, R. B. and Chuong, C.-M.: Wnt3a gradient converts radial to bilateral feather symmetry via topological arrangement of epithelia, *Proceedings of the National Academy of Sciences*, Vol. 103, No. 4, pp. 951–955 (online), DOI: 10.1073/pnas.0506894103 (2006).

[16] Yue, Z., Jiang, T. X., Wu, P., Widelitz, R. B. and Chuong, C. M.: Sprouty/FGF signaling regulates the proximaldistal feather morphology and the size of dermal papillae, *Developmental Biology*, Vol. 372, No. 1, pp. 45–54 (online), DOI: 10.1016/j.ydbio.2012.09.004 (2012).

[17] Zhang, F., Jiang, L. and Wang, S.: Repairable cascaded slide-lock system endows bird feathers with tear-resistance and superdurability, *Proceedings of the National Academy of Sciences*, Vol. 115, No. 40, pp. 10046–10051 (online), DOI: 10.1073/pnas.1808293115 (2018).

© 2019 Information Processing Society of Japan